

Wright State University

CORE Scholar

Computer Science and Engineering Faculty
Publications

Computer Science & Engineering

2011

3D Reconstruction of Human Ribcage and Lungs and Improved Visualization of Lung X-Ray Images through Removal of the Ribcage

Christopher Koehler

Thomas Wischgoll

Wright State University - Main Campus, thomas.wischgoll@wright.edu

Follow this and additional works at: <https://corescholar.libraries.wright.edu/cse>



Part of the [Computer Sciences Commons](#), and the [Engineering Commons](#)

Repository Citation

Koehler, C., & Wischgoll, T. (2011). 3D Reconstruction of Human Ribcage and Lungs and Improved Visualization of Lung X-Ray Images through Removal of the Ribcage. *Dagstuhl Follow-Ups*, 2, 176-187. <https://corescholar.libraries.wright.edu/cse/305>

This Article is brought to you for free and open access by Wright State University's CORE Scholar. It has been accepted for inclusion in Computer Science and Engineering Faculty Publications by an authorized administrator of CORE Scholar. For more information, please contact library-corescholar@wright.edu.

3D Reconstruction of Human Ribcage and Lungs and Improved Visualization of Lung X-ray Images Through Removal of the Ribcage

Christopher Koehler¹ and Thomas Wischgoll²

- 1 Wright State University
3640 Col. Glenn Hwy, Dayton OH 45431
koehler.11@wright.edu
- 2 Wright State University
3640 Col. Glenn Hwy, Dayton OH 45431
thomas.wischgoll@wright.edu

Abstract

The analysis of X-ray imagery is the standard pre-screening approach for lung cancer. Unlike CT-scans, X-ray images only provide a 2D projection of the patient's body. As a result occlusions, i.e. some body parts covering other areas of the body within this projected X-ray image, can make the analysis more difficult. For example, the ribs, a predominant feature within the X-ray image, can cover up cancerous nodules, making it difficult for the Computer Aided Diagnostic (CAD) systems or even a doctor to detect such nodules. Hence, this paper describes a methodology for reconstructing a patient-specific 3D model of the ribs and lungs based on a set of lateral and PA X-ray images, which allows the system to calculate simulated X-ray images of just the ribs. The simulated X-ray images can then be subtracted from the original PA X-ray image resulting in an image where most of the cross hatching pattern caused by the ribs is removed to improve on automated diagnostic processes.

1998 ACM Subject Classification J.3 Life and medical sciences, I.3 Computer graphics, I.3.7 Three-Dimensional Graphics and Realism

Keywords and phrases 3D Reconstruction, X-ray images

Digital Object Identifier 10.4230/DFU.Vol2.SciViz.2011.176

1 Background

Lung cancer accounts for more cancer deaths in the United States than any other form of cancer [5]. Unfortunately, the chances of surviving lung cancer drop drastically if it is not detected early enough. 3D CT scans are a more effective visualization technique for detecting lung cancer than X-ray images [6], however they – besides a significantly higher dose of radiation, are very expensive in comparison to use for early screening of patients who do not know if they have the disease. For this reason, traditional PA and lateral X-ray images are still the most used method for lung cancer early detection. A PA X-ray image is taken from behind a patient and shows the posterior (rear) and anterior (front) portion of the ribs, whereas a lateral X-ray image is taken from the side of a patient.

Computer aided disease detection (CAD) software is an effective tool to aid medical professionals in the difficult task of detecting lung cancer at its early stages in X-ray images. Typically CAD software focuses on the PA X-ray images, and uses image processing and soft computation techniques to identify potentially diseased areas. However, the anatomy of the upper body, such as the ribs, can obscure some of the cancerous nodules making it



© C. Koehler and T. Wischgoll;

licensed under Creative Commons License NC-ND

Scientific Visualization: Interactions, Features, Metaphors. *Dagstuhl Follow-Ups, Vol. 2.*

Editor: Hans Hagen; pp. 176–187



Dagstuhl Publishing

Schloss Dagstuhl – Leibniz Zentrum für, Germany

difficult for the CAD software to detect such nodules. Hence, removing the ribs beforehand can improve the overall result.

It would be ideal to be able to use the available X-ray images that are already being collected to generate an approximate 3D reconstruction of the ribs and lungs and then use the final reconstructed geometry to remove the ribs from the original X-ray image. This paper presents a unique approach for generating such a reconstruction that combines the user's knowledge of the general shape of human ribs and lungs with X-ray image segmentations and 3D geometric templates to generate patient specific ribcage and lung reconstructions. Furthermore, the final reconstructions are voxelized and subtracted from the PA X-ray image in order to remove the ribs, thereby allowing a user to see the lungs more clearly.

2 Related Work

There have been several techniques presented in the literature for creating 3D reconstructions based on X-ray image data. Statistical shape models and atlases were used to reconstruct a 3D pelvis based on two X-ray images [8]. Several techniques focusing specifically on creating ribcage reconstructions to aid in treatment of patients with scoliosis have also been presented. Patient specific scoliotic 3D bone models were generated based on free form deformation, one lateral X-ray image and two PA X-ray images taken at different angles [3]. Also, X-ray image based reconstructions were done for scoliosis patients by using an energy minimization function to select from a database of probabilistic prior models. While the application is entirely different, the techniques to reconstruct buildings in 3D based on architectural drawings described by Yin et al. [16] also have a lot in common with reconstructing anatomical structures based on X-ray images. More recently, Dworzak et al. reconstructed the human ribcage from a set of two images based on a statistical shape model [4].

For segmenting the rib borders in PA X-ray images, several techniques have been proposed by other researchers. Multiple vertical portions of X-ray images have been mapped to sinusoidal functions to detect rib edges [11]. Approximate rib borders have been found with the Hough transform and then refined with R-Snakes [17]. Statistical ribcage models have been aligned to patient specific data [15]. Iterative pixel classification has also been used to segment rib borders [9]. Semi-automatic segmentation of both the anterior and posterior ribs has been achieved with directional filtering and parallel edge following [10]. Since it is the only published algorithm capable of segmenting entire ribs in PA X-ray images, the technique described in [10] was used to generate segmentation data to test our reconstruction algorithms.

Our lung reconstruction algorithm is based on interactively refining the Boolean intersection of the convex hull of a reconstructed ribcage and a 3D extrusion of the lung fields detected in the PA X-ray image. Thus, a reliable method for segmenting the lungs is a necessary part of the reconstruction process. There have been several methods to segment lung fields presented in the literature in the last several years. Adaptive-sized hybrid neural networks were used to classify pixels as being part of a lung or not based on measurements taken at that pixel [13]. A combination of pixel classification and rule-based segmentation has also been effectively used to segment lung fields in X-ray images [14].

3 Rib Subtraction

One promising application of a 3D reconstruction of the ribs and lung fields is to subtract the ribs from the original X-ray images. The rib subtraction algorithm utilizes knowledge gained

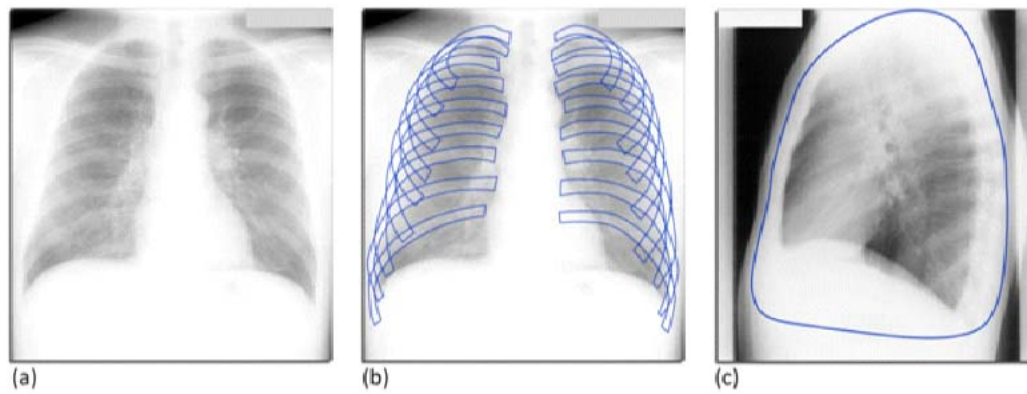
during both the segmentation and reconstruction processes. The goal of the algorithm is to reduce intensities at pixels which correspond to ribs in the original PA X-ray image in order to significantly reduce the confusing cross-hatching pattern that the ribs leave in the images without altering any other data contained in the image. The algorithm consists of several steps. First, the 3D reconstructions of both the ribs and the lung fields have to be generated based on a patient specific set of X-ray images. For this, the ribs and lung fields have to be segmented within the X-ray images. Based on these results, a 3D geometric representation of the ribs and the lung fields can be derived. Using these geometric representations, an X-ray image can be simulated that only contains a projection of the ribs by emulating the way an X-ray would transverse the ribs and the lung fields. This simulated X-ray image is then subtracted from the original PA X-ray image, thereby removing the majority of the rib silhouettes from that image. This cleaned up image can then be used for further diagnostic processing, such as analysis using CAD software. The individual steps of the algorithm are discussed in more detail in the following sub-sections.

3.1 Segmentation

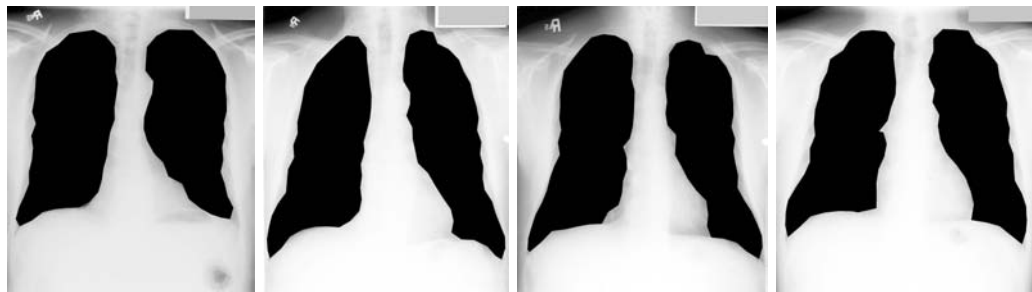
The algorithms to reconstruct both the ribs and the lungs involve alignment of 3D models to 2D segmentation data from the X-ray images and also generation of 3D meshes by extruding certain 2D features found in the images. Hence, it is important to start with accurate segmentations of the X-ray images. In particular it is necessary to segment the lung fields and the rib borders in the PA X-ray image, and the outer border of the ribcage in the lateral X-ray image. Segmenting anatomical features in 2D X-ray images is a difficult task due to the large genetic variations between patients as well as the subtle intensity variations resulting from bone, organs and soft tissue being superimposed onto each other during the X-ray process. Our solution is to use a combination of both automated and interactive segmentation techniques that integrate some of the best features of previously published segmentation work with our own unique algorithms to detect all necessary features from a pair of X-ray images.

The segmentation of the rib borders is based on the approach by Plourde et al. [10]. The 3D reconstruction process also requires some data about the rib structure from the lateral X-ray image. Lateral X-ray images can be extremely difficult to interpret due to ribs from both sides of the patient as well as the vertebrae all being superimposed on top of each other, so a completely automated segmentation is not feasible due to the high amount of intuition required for this task. However, since the general shape of a rib is known ahead of time, it is only necessary for a technician to interactively identify one point from each rib along the rear border of the ribcage and one point on the front border in the lateral X-ray image. A b-spline curve is used to interpolate between the marked points, which forms an approximate segmentation of the ribcage boundary. A local window of histogram equalization and contrast adjustment follows the user's mouse cursor throughout the process to make it easier to identify ribs in the noisiest portions of the image. The results of the rib segmentations are shown in Figure 1.

In order to eliminate the ribs from the PA X-ray image, an accurate reconstruction of the lung fields is needed in addition to the segmented ribs. The lung fields appear as two large dark patches in the center of the images, surrounded by a lighter area due to the lateral ribs, shoulder bones, organs and soft tissue. The corners of PA X-Ray images are often dark due to the patient's bodies not extending to the image corners. The first step of the lung segmentation algorithm is to identify pixels near the center of both lungs, separate approximate lung field boundaries from any other dark patches in the image and then later



■ **Figure 1** Rib segmentation process and results. (a) Initial PA X-ray image. (b) Segmentation done based on Plourde's edge following method. (c) Ribcage boundary segmentation.



■ **Figure 2** Lung segmentation for four different patient data sets.

attempt to refine the segmentation border.

As a starting point, the average pixel intensity in the PA X-ray image is taken as a threshold value. All pixels below this threshold are marked black and all those above are marked white. Then, image intensities are examined along every scan line of the image; white pixels closest to its center are assumed to be on the spinal cord and black pixels to the left and right of this white area are assumed to belong to the lung fields. The threshold value is gradually reduced until there are no longer any paths of black pixels from the lung field centers to the image borders. All black pixels that are connected to the image borders are then set to white. To smooth the lung borders and to remove any remaining noisy spots in the image, Gaussian smoothing is performed with a large value of sigma, and thresholding is done again resulting in another binary image. Any remaining black patches except the two largest are then removed.

Based on this segmentation, a contour line is generated consisting of a series of connected vertices which are refined to more closely match the true lung boundaries using Canny edge detection [2]. The contours are then recursively traced and discretized into a series of vertices. The bottom inner portions of the discretized lung segmentations are refined with an active contour based technique. The slope of the tangent at each discretized vertex is taken as the slope of the line between the next and previous vertices. The negative inverse of the slope is then used to find endpoints of a line segment orthogonal to the current pixel and the endpoints are connected. The intensities of the original PA X-ray image underlying each point on this new line segment are found resulting in an intensity histogram, which is smoothed with a Gaussian kernel. The first derivatives of the intensity histogram are

computed. The pixel with the maximum rate of intensity change is assumed to be part of the new discretized boundary of the lung field if the intensity change at that pixel exceeds a threshold. Parameters such as this threshold, the length of the orthogonal line segments, and the smoothing filter kernel size were determined experimentally in order to achieve the closest match with expert segmentations. Figure 2 shows results of the lung segmentation and discretization process for four different sets of X-ray images.

3.2 3D Reconstruction

The ribcage is reconstructed first based on our previous work [7]. Using a rib template of the shape of a half-torus, the geometry of the individual ribs is reconstructed by moving the vertices of the template to line up with the projections as defined by the segmentation results of the lateral and PA X-ray images. The basic idea is to exploit the fact that the overall shape of a rib is known. Hence, this shape, represented by the rib template, has to be matched with the segmentation found in the X-ray images. Specifically, the template is split up into clusters of vertices, where each of these clusters forms a ring around the rib. These clusters are first moved to match the location of the corresponding rib within the PA X-ray image. In a second step, the clusters of vertices are aligned with the segmentation results of the lateral X-ray image. This then results in a geometric representation of each rib as shown in the first row of Figure 4.

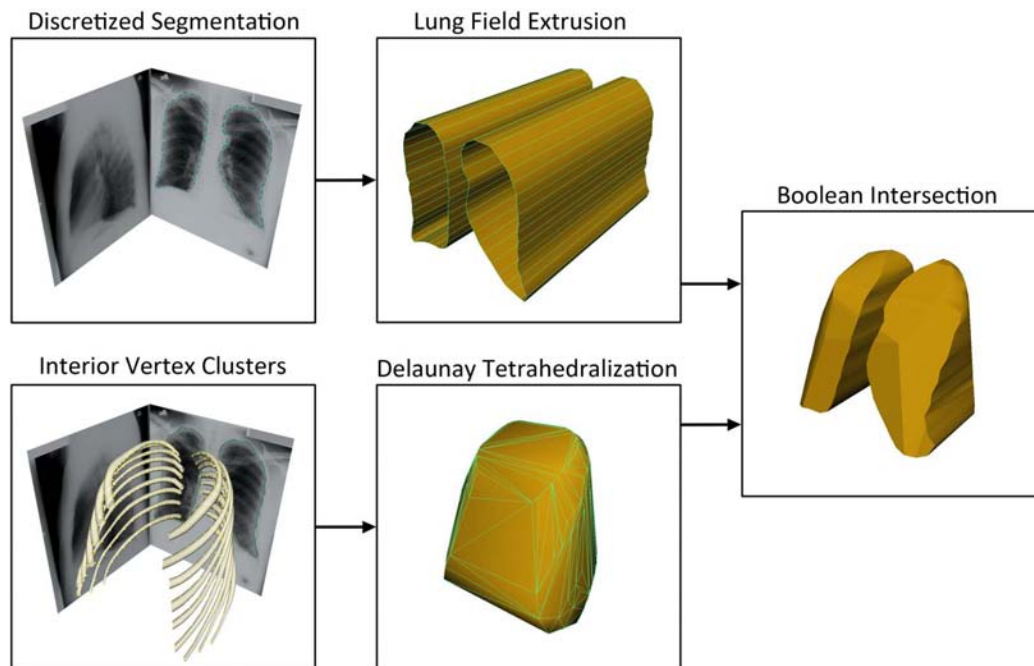
The geometric lung reconstruction utilizes both the rib reconstruction data that has already been generated and the lung segmentation data. Essentially it works by creating a mesh that encompasses the inside of the reconstructed ribcage, and then carves out the portion of that mesh which corresponds to the lungs by extruding the segmented lungs up through it. The resulting mesh is then refined with polygon reduction and subdivision smoothing so that its surface is smooth like that of a real lung.

Earlier in the section on lung segmentation, it was mentioned that the segmentation boundary was discretized into a series of vertices. The reason for doing this is that those vertices can now be extruded into 3D to generate a shape that is the basis for reconstructing the lungs. The result is two tube-like structures that resemble lungs from the front, but are completely flat along the sides. The reason for choosing a discretization interval that is coarser than the available accuracy of the segmentation is that it would create a mesh with many extremely skinny triangular faces later when it is merged with another mesh whose accuracy is already limited by a lack of data between ribs.

True lungs do not have flat sides, but rather they curve along with the interior of the ribs. The extrusion of the lung fields alone does not capture this fact, and there is no data that can be taken directly from the X-ray images to generate this structure. What can be used is the reconstructed ribcage that has already been generated at this point. Vertices along the interior of each reconstructed rib are found and a new mesh is generated that fills the interior of the ribcage by computing the Delaunay tetrahedrization [12] [1] of these vertices.

The new mesh resulting from the Delaunay tetrahedrization captures approximately how the outer border of the lungs follow the inside of the ribcage, but it is solid in the center and near the bottom where the trachea, diaphragm, vertebrae and heart should be located. The silhouette of these features shows up white in the PA X-ray image so they are not included in the lung segmentation. Thus, the next step of the lung reconstruction is to carve the lung fields out by taking the Boolean intersection of the two meshes. The lung reconstruction process up to this point is illustrated in Figure 3.

The initial reconstructed lung mesh contains hard edges at the boundaries of where the ribcage interior and lung extrusion meshes intersected each other. This can be fixed through



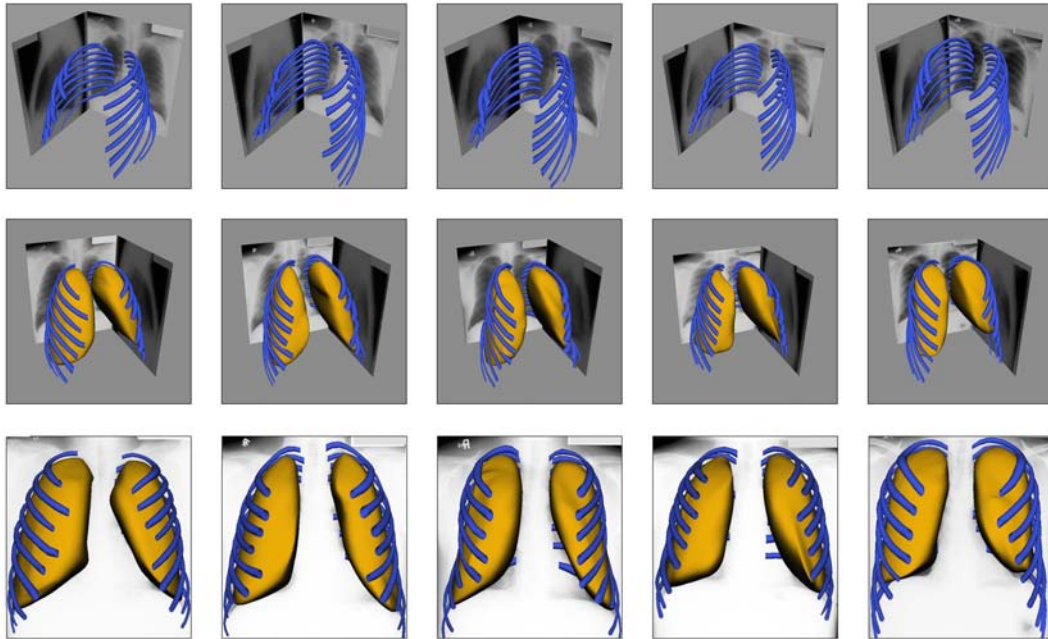
■ **Figure 3** Initial lung reconstruction process. Top: The discretized lung segmentation is extruded into two hollow lung fields. Bottom: A polygon mesh is generated by taking the Delaunay tetrahedralization of the interior vertex clusters of each rib after the rib reconstruction is complete. Right: The initial reconstructed lung meshes are created by taking the Boolean intersection of the extruded lung fields and the Delaunay tetrahedralization.

a combination of polygon reduction and subdivision smoothing. This process is not entirely straightforward though because despite our best efforts to limit it at several steps in the reconstruction, there will inevitably be a variable number of strangely shaped polygons in the initial mesh of the reconstructed lungs. Subdivision smoothing alone produces undesirable results due to the high variation in the faces of the mesh. Even with polygon reduction performed first to make the faces more uniform, artifacts of the reconstruction process will manifest themselves in the final smoothed model for variable percentages of polygon reduction, making it difficult to hardcode a set reduction percentage. Hence, the current software allows for some user intervention at this point ensuring an optimal choice to yield an appropriate reconstruction of the lung volume.

The rib and lung reconstructions as well as the segmentation methods were tested on 19 pairs of PA and lateral X-ray images. Results from four of the patients with significantly different bone structures are shown from several views in Figure 4. In the future we hope to further validate the results of the lung reconstruction algorithm against a CT scan of a human torso by creating simulated X-ray images through volume renderings, performing rib and lung reconstructions and then comparing the results to the original CT.

3.3 X-Ray Simulation

To get an estimate of how much intensity should be subtracted from each pixel in the original X-ray images, simulated X-ray images of both the ribs and the lungs are generated. In order to create X-ray simulations, the polygon based meshes created by the rib and lung

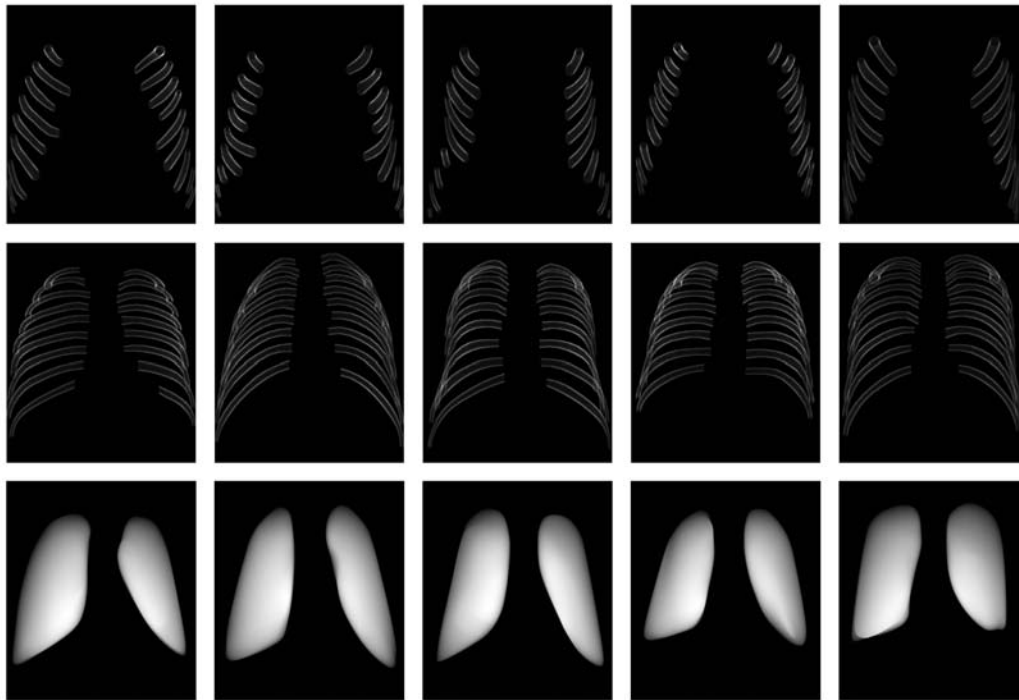


■ **Figure 4** Renderings of final output from the rib and lung reconstruction algorithms when used on four different patients with significantly different bone structures rendered from the front, back, and two other angles.

reconstruction are first converted to voxels. For this, the geometric description of the ribs is discretized into voxels at the same resolution as governed by the input X-ray image dimensions such that every triangle in the reconstructed mesh is covered by a voxel in the resulting volumetric space. Volume renderings are then created from the voxelized reconstruction to simulate X-raying the reconstructed ribs and lungs. In order to remove any artifacts of the reconstruction, voxelization and volume rendering processes, Gaussian blurring is performed on the renderings. Then they are clipped against the original rib segmentations. These cleaned renderings are then weighted and subtracted from the original X-ray images, which effectively removes most of the ribs from the X-ray images.

The interior of the voxelized lungs was filled prior to rendering them however, the ribs are intentionally not filled after they are converted to voxels so that the edges of the rendered ribs will be lighter in order to capture the effects of real bones when they are X-rayed. Bone is porous on the inside, but much denser toward its surface, thus more intensity needs to be subtracted from the bone edges to remove them from the images. This effect can be seen in Figure 5.

A rib removal scheme needs to ensure minimal alterations of the original lung data in the X-ray images and not just softening the effect of the ribs. Intensity subtraction based on the rendering of the voxelized rib and lung reconstruction data helps achieve both of these goals. Rib removal is only done inside the original lung segmentations because the lungs are the most important part of the PA X-ray images for applications like disease detection, so it is not important to remove the lateral ribs as nothing of interesting is located behind them as far as detecting cancerous nodules is concerned.



■ **Figure 5** Simulated X-ray renderings of the anterior (top), posterior (center), and lungs (bottom).

3.4 Rib Splitting

Since the effect of the anterior portion of the ribs in the original X-ray images is very subtle, they are rendered separately from the posterior ribs by splitting the reconstructed rib meshes into posterior and anterior portions before they are voxelized (Figure 5). In order to reduce the intensities of each pixel in the anterior rib rendering, it is desirable to know how thick the lung would have been at that pixel. This is what the simulated lung X-ray image mentioned in the previous section is used for. The anterior rib subtraction process is the same as what is done for the posterior ribs; however, their effect is reduced proportionally to the intensity of the lung X-ray simulation at each pixel and a different user controlled weight is applied to them. These renderings are weighted and subtracted from the original X-ray images, which effectively removes the ribs from the X-ray images.

One side effect from both the posterior and anterior rib removal is a slight dark boundary around where the ribs used to be. This is due to a partial pixel effect combined with slight inaccuracies in the original segmentation of the ribs. Despite this side effect, the overall result reduces the effect of the ribs in the PA X-ray image and makes it easier to get a better look at the lungs. Pairs of PA X-ray images for four patients are shown before and after rib subtraction in Figure 6.

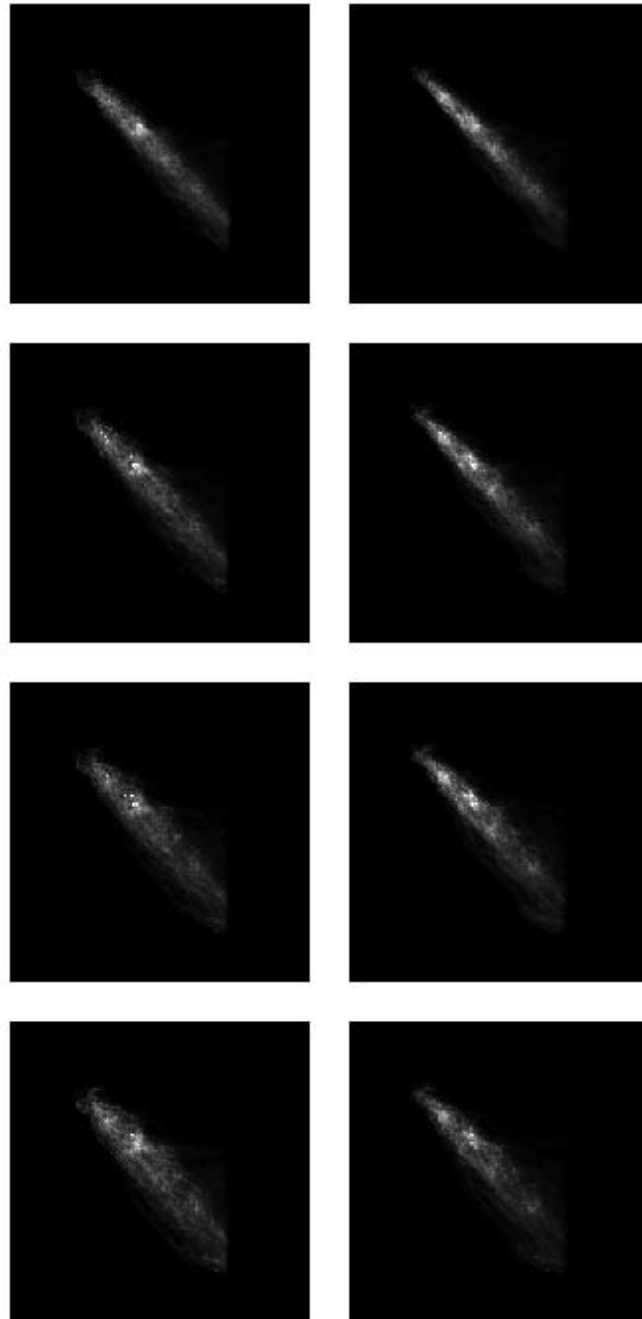
3.5 Automation

To get the best results in the rib removal, a technician adjusts two sliders controlling the weights applied to the posterior and anterior rib renderings before subtraction. This process can be done in under a minute so it is not a hindrance, but preliminary experiments have been done on how to automatically generate the best rib subtraction images.



■ **Figure 6** Original (left) and X-ray images with ribs subtracted (right).

Second-order gray-level statistics were chosen as a starting point to automatically discern the quality of a rib subtraction due to the fact that they can look at pairs of pixels that are both inside and outside of a rib. In order to compare second-order gray-level statistics before and after the rib subtraction, the co-occurrence matrix of each image must be generated. The co-occurrence matrix $H(m, n)$ is defined as the number of image locations (r, c) for which the corresponding pixel has intensity m and the pixel at location $(r + \Delta r, c + \Delta c)$ has intensity n .



■ **Figure 7** Intensity co-occurrence matrices before (left) and after (right) rib-removal for four different values of Δr .

The co-occurrence matrices generated from before and after rib subtraction for one patient are shown in Figure 7. The individual images show the matrix before (left) and after the removal of the ribs (right). In each pair Δc was set to 0 while Δr is incremented, because the rows occupied by a single rib does not change greatly at any portion of the rib. The values of Δr were chosen in hopes of maximizing the number of pixel pairs where one pixel was inside a rib and one pixel was not. Only intensities that were inside the segmented lungs

were used in this step to prevent the very light lateral ribs and the very dark background from throwing off measurements. The co-occurrence matrix should depict mainly diagonal entries when there is little intensity variation in the measured image. As can be seen from the images, there is a slight improvement in that the light diagonal strip shown in the images becomes slightly thinner and more distinct in the matrices on the right side of Figure 7. However, all the second-order grey level statistics based on these co-occurrence matrices tested thus far, such as energy, entropy, correlation and contrast, have been insufficient to automatically discern the quality of a rib removal, so more work is needed in this area to achieve a fully automated approach.

4 Conclusion

We have developed an algorithm that generates geometric reconstructions of the ribs and lungs based on a pair of PA and lateral chest X-ray images by combining segmentation and geometric templates. Using the geometric reconstructions of the ribs and lungs, simulated X-ray images can be generated and subtracted from the original PA X-ray images to eliminate the ribs. This then can help in the diagnostic process where ribs overlaying cancerous nodules may result in misdiagnosis when analyzed by a physician or using computer aided detection software.

Medical professionals will ultimately evaluate whether such reconstruction techniques are useful as a supplement to increase the accuracy of current disease detection methods. Any technique that can add even a small percentage decrease in the number of false positive and false negative diagnoses is of great value, which is where the removal of the ribs can help by reducing the effect of obstructing anatomic elements on the detection of cancerous nodules.

Acknowledgments

The authors thank Riverain Medical for providing the data sets used in this paper as well as the Ohio Department of Development and the Dayton Area Graduate Studies Institute (DAGSI) for providing funding for the Early Lung Disease Detection Alliance to pursue the presented research agenda.

References

- 1 Joe Barry. Construction of three-dimensional Delaunay triangulations using local transformations. *Comput.Aided Geom.Des.*, 8(2):123–142, 1991.
- 2 John Canny. A Computational Approach to Edge Detection. *IEEE Transactions on Pattern Analysis and Machine Intelligence*, PAMI-8(6):679–698, 1986.
- 3 S. Delorme, Y. Petit, J. A. de Guise, H. Labelle, C. E Aubin, and J. Dansereau. Assessment of the 3-D reconstruction and high-resolution geometrical modeling of the human skeletal trunk from 2-D radiographic images. *IEEE Transactions on Biomedical Engineering*, 50(8):989–998, 2003.
- 4 J. Dworzak, H. Lamecker, J. von Berg, T. Klinder, C. Lorenz, D. Kainmu"ller, H. Seim, H. C. Hege, and S. Zachow. 3D reconstruction of the human rib cage from 3D projection images using a statistical shape model. *International Journal of Computer Assisted Radiology and Surgery*, 2009.
- 5 Centers for Disease Control and Prevention. Cancer – Lung Cancer Statistics, January 7 2009.

- 6 M. Kaneko, K. Eguchi, H. Ohmatsu, R. Kakinuma, T. Naruke, K. Suemasu, and N. Moriyama. Peripheral lung cancer: screening and detection with low-dose spiral CT versus radiography. *Radiology*, 201(3):798–802, December 1 1996.
- 7 C. Koehler and T. Wischgoll. 3-d reconstruction of the human ribcage based on chest x-ray images and template models. *IEEE MultiMedia*, 17(3):46–53, 2010.
- 8 Hans Lamecker, Thomas H. Wenckebach, and Hans-Christian Hege. Atlas-based 3d-shape reconstruction from x-ray images. *International Conference on Pattern Recognition*, 1:371–374, 2006.
- 9 M. Loog and B. Ginneken. Segmentation of the posterior ribs in chest radiographs using iterated contextual pixel classification. *IEEE Transactions on Medical Imaging*, 25(5):602–611, 2006.
- 10 F. Plourde, F. Cheriet, and J. Dansereau. Semi-automatic detection of scoliotic rib borders using chest radiographs. *Studies in Health Technology & Informatics*, 123:533–537, 2006.
- 11 Shigeru Sanada, Kunio Doi, and Heber MacMahon. Image feature analysis and computer-aided diagnosis in digital radiography: Automated delineation of posterior ribs in chest images. *Med.Phys.*, 18(5):964–971, September 1991 1991.
- 12 Hang Si. TetGen: A Quality Tetrahedral Mesh Generator and Three-Dimensional Delaunay Triangulator. howpublished: <http://tetgen.berlios.de/>.
- 13 Osamu Tsujii, Matthew T. Freedman, and Seong K. Mun. Automated segmentation of anatomic regions in chest radiographs using an adaptive-sized hybrid neural network. *Medical physics*, 25(6):998–1007, 1998.
- 14 B. van Ginneken and B. M. ter Haar Romeny. Automatic delineation of ribs in frontal chest radiographs. *Proceedings of SPIE – The International Society for Optical Engineering*, 3979:825–836, 2000.
- 15 Bram van Ginneken and Bart M. ter Haar Romeny. Automatic segmentation of lung fields in chest radiographs. *Medical physics*, 27(10):2445–2455, 2000.
- 16 Xuetao Yin, P. Wonka, and A. Razdan. Generating 3D Building Models from Architectural Drawings: A Survey. *Computer Graphics and Applications, IEEE*, 29(1):20–30, 2009.
- 17 Zhanjun Yue, A. Goshtasby, and L. V. Ackerman. Automatic detection of rib borders in chest radiographs. *IEEE Transactions on Medical Imaging*, 14(3):525–536, 1995.